OMAE2020-18030

ANALYSIS OF OPEN-SOURCE CFD TOOLS FOR SIMULATING COMPLEX HYDRODYNAMIC PROBLEMS

Mohd Atif Siddiqui [*]
Marine Technology Dept.,
NTNU
Trondheim, Norway
Email: mohd.a.siddiqui@ntnu.no

Marilena Greco
Marine Technology Dept., NTNU
Trondheim, Norway
CNR-INM, Inst. of Marine Eng.,
Rome, Italy

Hui-li Xu
Marine Technology Dept.,
NTNU
Trondheim, Norway
Email: hui-li.xu@ntnu.no

Giuseppina Colicchio
Marine Technology Dept., NTNU
Trondheim, Norway
CNR-INM, Inst. of Marine Eng.,
Rome, Italy

ABSTRACT

OpenFOAM (OF) represents an attractive and widely used open-source environment for simulating complex hydrodynamic scenarios with several implemented numerical methods and wide variety of problems it can be applied to. For commercial and open-source solvers, though, expertise and experience are required to get physical and reliable results. Here, without pretending to be exhaustive, we aim to contribute in highlighting advantages and challenges of some key computational fluid dynamics (CFD)-simulation tools, with focus on the OF platform. We examine the effect of grid type, grid size and time-evolution scheme. Dynamic-mesh techniques and their influence on local and global numerical results are discussed, as well as the use of an overset grid versus a deforming mesh. Lastly, possible error sources in CFD simulations are discussed. These numerical studies are performed investigating two complex hydrodynamic problems: 1. a fully-immersed flapping hydrofoil aimed to generate thrust, 2. a damaged and an intact ship section fixed in beam-sea waves, in forced heave and roll motion in calm water. In the first case, vortex-shedding and wake features are crucial; in the second case, free-surface flow effects play the key role while the importance of vortex-shedding and viscous-flow effects depends on the scenario. The first problem is solved with OF and validated with results from benchmark experiments. The second problem is solved using (A) OF, (B) an in-house CFD solver and (C) a fully-nonlinear potential-flow code. A and B assume laminar-flow conditions and use, respectively, a volume-of-fluid and a level-set technique to handle the free-surface evolution. C is considered to examine importance of nonlinear versus viscous effects for the examined problems. The results are compared against in-house experiments.

Keywords: CFD, Grid strategies, Flapping foil, Damaged ship hydrodynamics, Vortex shedding, Numerical Wave Tank

NOMENCLATURE

a_{33}:	Heave added mass
b_{33}:	Heave damping
c:	chord length
f :	frequency of forced oscillations (Hz)
A :	amplitude of forced oscillations (m)
ALE:	Arbitrary Lagrangian Eulerian
A_r :	submerged cross-section area (m^2)
A_D :	amplitude-to-body length ratio $A_D = A/D$
B:	Breadth of the damaged/intact model
BEM:	Boundary element method
BH:	Block Hex grid
C_d :	Drag coefficient
C_l :	Drag coefficient
CN :	Crank-Nicholson scheme
D :	characteristic body/foil length (m)
DM:	Deforming mesh
F_3:	Heave force per unit length
LS:	Level Set
NS:	Navier-Stokes
NWT:	Numerical wave tank
OF:	OpenFOAM
OG:	Overset Grid
Re_c :	Reynold's Number $Re_c = U_c D / \nu$
Sr :	Strouhal Number $Sr = fD/U_c$
T:	Incident wave period (s)
T_d:	Draft of the damaged/intact model
U_c :	uniform inflow velocity (m/s)
VOF:	Volume of fraction method
ρ :	Density of fluid (Kg/m^3)
ν :	Kinematic viscosity of fluid (m^2/s)

1 INTRODUCTION

The modern availability of large computational power has driven the surge in usage of CFD in hydrodynamic studies. It has been extensively applied for studying ship drag/resistance, wake behind propellers, hydrofoils and flow around local geometries (roll damping fins/anti-roll sloshing tanks). The focus of these studies is to optimize ship geometry and reduce drag/optimize design parameters. Many of these problems are solved using single-phase Navier-Stokes (NS) solvers with fully submerged bodies and uniform inflow velocity boundary conditions. CFD methods have also recently been applied to study two-phase flow problems involving fluid-structure interaction (FSI) and/or wave propagation. Generally potential flow codes are employed for analyzing seakeeping problems incorporating empirical damping models to include viscous-flow effects. However, with ever increasing computer speeds, CFD models have become more popular in the last few years. Commercial software is relevant for use in industrial applications but can be costly and difficult to modify for specific user requirements. Therefore, open-source CFD solvers like OF and REEF3D are attractive, especially among the research community. The former mostly uses the volume-of-fluid (VOF) method while the latter employs the level-set (LS) technique to capture the free-surface evolution. These solvers are particularly advantageous due to the availability of large number and type of utilities for pre-processing, solution and post-processing of CFD problems. In addition, easy implementation of user-defined routines makes them very valuable for developers and researchers.

Numerical wave tanks (NWT) incorporating viscous solvers have been successfully implemented for studying various hydrodynamic problems. Jacobsen et al. [1] presented a wave generation and absorption system using OF. They used two benchmark test cases, to demonstrate the ability of wave propagation. Bihs et al. [2] implemented a three-dimensional (3D) NWT in REEF3D for modelling of wave hydrodynamics. Windt et al. [3] and Miquel et al. [4] analyzed various methods available for development of NWTs in OF and REEF3D, respectively. For seakeeping applications, CFD have been used for estimating added mass and damping coefficients in recent studies as shown by Bonfiglio et al. [5] for two-dimensional (2D) ship shaped sections, Chen and Christensen [6] for cylinders and Thilleul et al. [7] for both 2D ship sections and cylinders. Added mass and damping coefficients for angular motions (roll/pitch) are the hardest to estimate accurately. In beam-sea waves, roll motion is significant and for its estimation, we need to calculate roll damping precisely. Some recent studies have tried to understand and highlight the best practices to calculate roll damping using CFD for intact ships (Jaouen et al. [8] and Mancini et al. [9]). The former used forced roll motions whereas the latter employed URANS (Unsteady Reynolds averaged solvers) simulation of roll decay for a freely-floating ship model in 3/6 degree of freedom (DOF) motion using overset grid technique.

For moving bodies/boundaries, the most common approach is to use Arbitrary Lagrangian Eulerian (ALE) scheme. The topology remains constant and the grid can distort to adapt to body motions. We refer to this approach as the deforming mesh (DM) in this paper. It can lead to large distortion of the cells in case of large motions, with the risk of substantial increase in the computational time or of numerical instability. Therefore, large motions are restricted. They can be handled by using overset (i.e. overlapping) grids (OG). In the scenario with two OGs, one

grid is fitted to the body and follows the rigid body motions, whereas the background grid remains fixed. This technique increases the computational time. One of the main aspects of this work is to analyze the effect of mesh motion techniques in OF on global and local results. This has been performed in works by Windt et al. [10] and Decorte and Monbaliu [11]. The former studied the performance of overset grids in OF for studying free decay of a wave energy converter, whereas the latter studied free heave decay of a 3D cylinder and heave motion in waves. Chen et al. [12] studied the use of overset mesh in OF for simulating a range of problems, including water entry of a wedge and motions of a lifeboat in head-sea waves. Following these works as inspiration, we apply DM and OG techniques in OF to study hydrodynamic problems involving moving rigid bodies, vortex-shedding and free-surface flows. The above-mentioned works compared numerical results with experimental results and/or DM and OG results. In addition to comparison with benchmark/new experiments, the focus is to study the effect of CFD parameters on local and global phenomena for both DM and OG techniques. We analyze the effect of time schemes, grid type and size on the results. Cost-benefit analysis is also discussed, wherever necessary, in terms of comparison error with experiments, computational effort/time required, effort in mesh generation, etc. Both single and two-phase solvers are considered to also analyze the effect on results for problems with air-water interface. Within this framework, we analyze two complex hydrodynamic problems. First, a submerged flapping foil used for thrust generation. Qualitative results are compared against benchmark experiments. Secondly, added mass, damping and diffraction forces on a 2D damaged ship section are calculated and compared against an intact section. For this case, we present comparison of diffraction results with a level-set NS solver (Colicchio et al. [13]), a potential-flow Boundary Element Method (BEM) code (Greco et al. [14]) and experiments (Siddiqui et al. [15]).

The paper is organized as follows. Section 2 discusses the studied hydrodynamic problems in brief. Section 3 provides a brief description of the numerical solvers along with mesh motion techniques and numerical schemes employed. Section 4 and 5 discuss the results and the numerical error sources, respectively, and section 6 provides relevant conclusions.

2 HYDRODYNAMICS OF STUDIED PROBLEMS
2.1 Flapping Foil

The high propulsive efficiency of fast speed aquatic animals has inspired research for understanding the thrust-generating mechanisms. The kinematics and dynamics of swimming fish is complex, but some key features can be grasped by using a simplified model of rigid flapping foils. Under proper configurations, flapping foils are associated with a reverse von Kármán wake and a time-averaged jet profile, and experiences thrust [16]. Andersen et al. [17], using a particle vortex method, argued that the drag–thrust transition occurs in a parameter region with wakes in which two vortex pairs are formed per oscillation period, in contrast to the common transition from a von Kármán to a reverse von Kármán wake. Numerical simulations performed using OF with an ALE formulation for the moving body and mesh, have shown satisfactory results compared with experimental data within an extended range of flapping parameters [18].

In this paper, we perform numerical simulations in order to replicate experiments from Godoy-Diana et al. [19]. They

performed forced angular motions (about O and z axis) of a foil as show in figure 1 in uniform inflow.
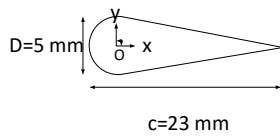

Figure 1. The foil parameters

The foil has a semi-circle section in the front and a triangular section in the aft.

2.2 Damaged versus intact ship section

Dynamic behavior of damaged ships in calm water or in waves differs significantly as compared to intact ships (see e.g., for roll motion in [20]). The lost in buoyancy coupled with sudden influx/outflux of floodwater through the damaged opening can result in large forces and movements. If subsequent capsize does not occur, usually a large heel and/or trim angle develop due to additional floodwater. Analysis of seakeeping/hydrodynamic behavior of damaged ships is, therefore, of great importance. It can, for example, help in the analysis of safe return to port.

In the present paper, we present results for experiments on an intact and damaged section (fig. 2) in a 2D wave flume. The model has an opening on the side, which is covered with a very thin watertight plate to simulate intact ship behavior. Here, the focus is on validation of and comparison with CFD results for the diffraction and radiation problems of an intact and a damaged ship model.
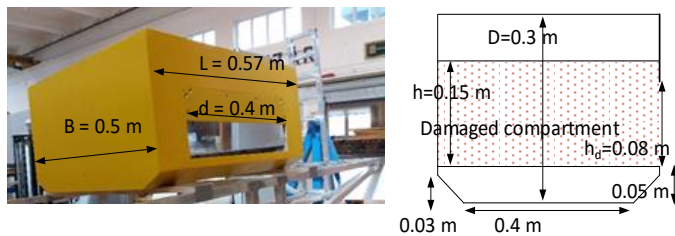

Figure 2. Damaged model during swing test (left) and front view illustration with dimensions (right)

The setup of diffraction-problem experiments, with the flume size and wave probe (WP) locations, is shown in figure 3. For the radiation problem, the setup is the same for the body and the beach on the right side. The wavemaker on the left is instead substituted by a numerical beach to damp out the radiated waves generated by the oscillating ship section. Finally, in this case only two wave probes (WP2 and WP4) are used; more details can be found in [15].
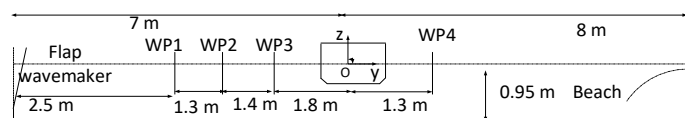

Figure 3. Diffraction-problem experimental setup

They are similar except for the wavemaker being replaced by a beach for the radiation problem. The width of the wave flume (x direction) is 0.58 m while the model size in that direction is 0.57 m. This setup helps to obtain predominantly 2D behavior in the experiments.

3 NUMERICAL SOLVERS

Here, we describe the main features of the OF solver used and related grid strategies, boundary conditions and other relevant aspects. A brief description of the solvers used for comparison is also provided.

3.1 OpenFOAM

A fully viscous single/two phase flow solver in OF versions 1806/1812 was employed for the numerical computations. Form of the governing equations and details of solution algorithms, solver settings and boundary conditions relevant for this work can be found in the user manual [21]. OF applies a finite volume discretization (FVD) technique on a collocated grid in the fluid domain. A second-order discretization is used in space for both the foil and ship sections. Use of first-order implicit Euler scheme, unbounded second-order, backward scheme and second-order, Crank-Nicholson scheme as time schemes will be examined. The pressure-velocity coupled equations are solved using the PIMPLE solver, which is a combination of PISO (Pressure Implicit with Splitting of Operator) and SIMPLE (Semi-Implicit Method for Pressure-Linked Equations). The inner (pressure correction for SIMPLE) and outer (pressure correction for PISO) iterations are set to 2 for all simulations as they give converged results. The transport equation for the VOF (α) function is solved using the MULES (Multidimensional Universal Limiter with Explicit Solution) solver. An adaptive time stepping method is employed to ensure stability by enforcing the maximum Courant number (Co) to be 0.3 for the foil case and 1 for the intact and damaged sections. The two-phase solver for the ship sections also requires an interface Courant number (Co_{pf}) which is set to 0.5. In addition, the initial and the maximum time step of the simulations are set to 0.0025 s, based on the average Co requirement. A variable time step is especially important for a deforming mesh scenario where mesh size changes in time and, therefore, the Courant number requirement varies with the mesh motion. For the foil case, the courant number never reaches the given maximum value, so all cases run at constant time step. For the ship sections, the time step usually varies and can reach small values as small as 1e-05 s in the beginning of the simulations but gradually reach constant values of around 0.0005-0.005 s depending on grid size and simulation parameters. The dynamic choice of the time step ensures stability of simulations and helps to avoid unphysical behavior in the NWT, especially at the beginning of simulations and when large mesh deformation occurs. The focus in this work is to analyze the effect of numerical parameters on the results while capturing the physics of the studied problem reasonably well. In this framework, we employed a laminar-flow solver for all simulations. This choice simplifies the numerical set up and appears reasonable due to the presence of nearly sharp corners for the intact and damaged ship sections. Similarly, the foil has a sharp trailing edge and the involved Reynolds number is sufficiently small to ensure laminar-flow separation along the body. However, one must note that, in real-flow conditions, the wake tends to become turbulent downstream of the body. This represents an error source of the numerical results. Additionally, all simulations are run on NTNU supercomputer VILJE nodes (Intel Xeon E5-2670), using 2 nodes (32 cores) per simulation.

3.1.1 Domain and boundary conditions

Flapping Foil A 2D computational domain is set up as shown in figure 4. A 2D simulation in OF implies that the third dimension is one cell thick and fluid properties are not solved for in this direction. The boundary conditions in this direction for all variables are, therefore, set to *empty* (not solved). The

domain length (x) and height (y) are set to –5.2c<x<6.5c and –3.25c<y<3.25c respectively, with c the chord length. The foil performs forced angular motions (*moving boundary condition*) about the origin and z axis. Along the foil, a no-slip (zero velocity) condition is enforced. A uniform inflow condition is given at the inlet and a uniform pressure condition at the outlet. To maintain uniform flow behavior, slip conditions are used on the top and bottom boundaries, i.e. only velocity in y direction is enforced to be zero. For the OG grid, an additional "overset" boundary condition for the interpolation layer is provided.
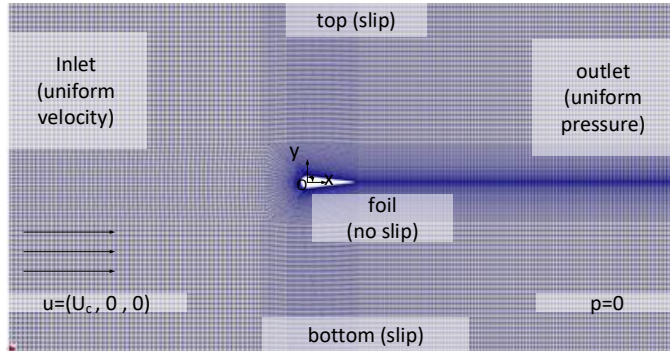
Figure 4. Computational domain for the flapping foil with enforced boundary conditions (C-grid shown here)

2D Ship Section In this case, a two-phase NWT is setup in OF. The NWT length and depth (fig. 5) are same as in the experiments (fig. 3). Figure 5 provides the boundary conditions for the diffraction problem and the contour plot of the volume fraction (α), with red shading indicating water ($\alpha=1$) and blue shading indicating air ($\alpha=0$).We perform 2D computations, so the direction in the plane of the paper is one cell thick, as described for the foil. The waves propagate from the left to the right side in the experiments and NWT. For the damaged section cases, the damage opening faces the incoming waves. A forced angular motion (*moving boundary condition*) about the hinge is given as input on the left end of the NWT. Here, the prescribed motion is the same of the experimental wavemaker. To implement a beach at the opposite end, waves are absorbed using the shallow-water absorption condition. This absorption method has been shown quite effective and details of this method for OF are presented by Higuera et al. [22]. A no-slip boundary condition is set at the bottom of the flume. At the top boundary (atmosphere), a fixed-value pressure condition is applied, i.e. total pressure is set to 0 (*constant*). The radiation problem is solved in a similar NWT but replacing the wave-maker with a damping zone similarly as at the opposite end. For the radiation problem, the body is given a prescribed oscillatory motion.
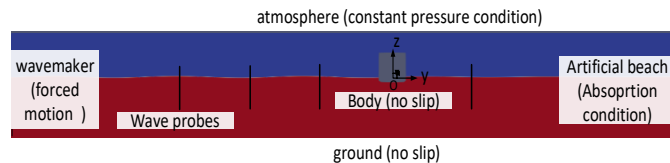

Figure 5. Computational domain for the 2D intact and damaged ship section diffraction problems, with enforced boundary conditions

For the forced roll motions, mesh distortion can be an issue, so we also employ an OG simulation. The body-fitted OG grid extends from -B<y<B, and -0.8B<z<0.7B, with B as defined in figure 2. The background grid domain size is as before. For x

direction, both OGs are one cell thick with an additional boundary condition for the overset layer.

3.1.2 Mesh Generation
Flapping Foil Two type of grids are used, as shown in figure 6. A C-grid is generated with ICEM© around the foil for the morphing mesh case, with 22800 structured hexahedral cells. For the overset case, the moving body fitted mesh is also generated using ICEM© and has 3640 hexahedral cells. Averagely, this gives a similar discretization size as for the C-grid near the body. The background mesh is generated using *blockMesh* utility (creating simple block hex grids) in OF. In our case, background mesh has 288000 cells (Δx=Δy= 0.000375 m). The overset mesh is constructed so that the outermost layer of the moving mesh has the same cell size as the background grid.
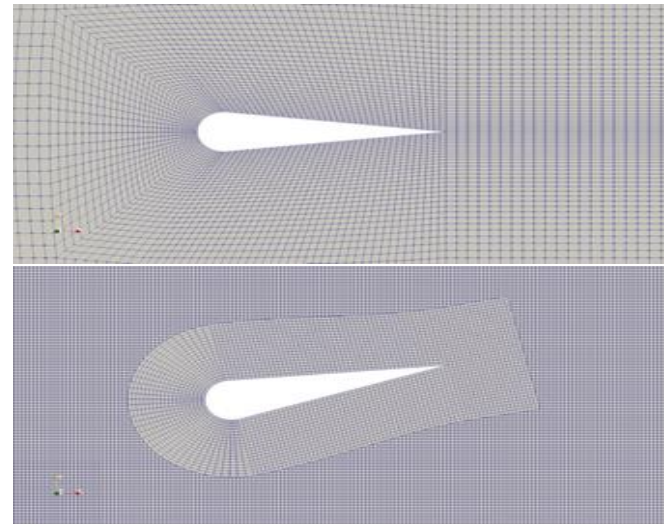

Figure 6. C type DM grid (top) and overset grid (bottom)

2D Ship Section For the diffraction and radiation problems with the DM technique, two types of grids are used, as shown in first and second plots of figure 7. The first is a structured block hexahedral (hex) (BH) grid generated using *blockMesh*. In our case, it involves three cell sizes, as discussed later. This mesh is highly refined near the free-surface (first plot of fig. 7). The second is an unstructured O grid generated using *snappyHexMesh* utility. This gives a body fitted grid with both hex and tetrahedral (tet) cells. However, it can only be created over a background grid generated with *blockMesh*, as shown in the second plot of figure 7. For forced roll motion of an intact section, a 2D DM simulation is performed with a structured O hex mesh (third plot of figure 7). In addition, a 2D overset grid simulation is performed. In this case, a 2D body-fitted mesh and the background mesh (both structured hex) are generated using *blockMesh,* as shown in the fourth plot of figure 7. The mesh size for the body-fitted and the background mesh are described later.

3.1.3 Mesh Motion
All the studies problems involve moving bodies/boundaries. Various deforming mesh techniques and their implementation in OF are discussed by Jasak and Tukovic [23]. The mesh motion for the entire domain is handled by solving $\nabla \cdot (k \nabla d) = 0$. Here, *k* is a diffusivity coefficient and *d* is the motion displacement vector for each cell. We use a quadratic distance-based diffusivity coefficient ($k = 1/r^2$), with *r* the

Copyright © 2020 ASME

cell-center distance from the specified moving boundary. This implies that as we go far away from the specified patches, less deformation occurs. However, when the moving boundary undergoes large motions, mesh distortion can affect accuracy and stability. To avoid severe mesh deformation for simulation of large body motions, an overset grid technique can be used. Here, we consider two grids. Fluid equations are solved on both grids and interpolation techniques are used for information exchange between the grids. As an example, figure 8 shows the body covered (hole) region in red, where no equations are solved, and the interpolation layer for the body-fitted grid in grey.
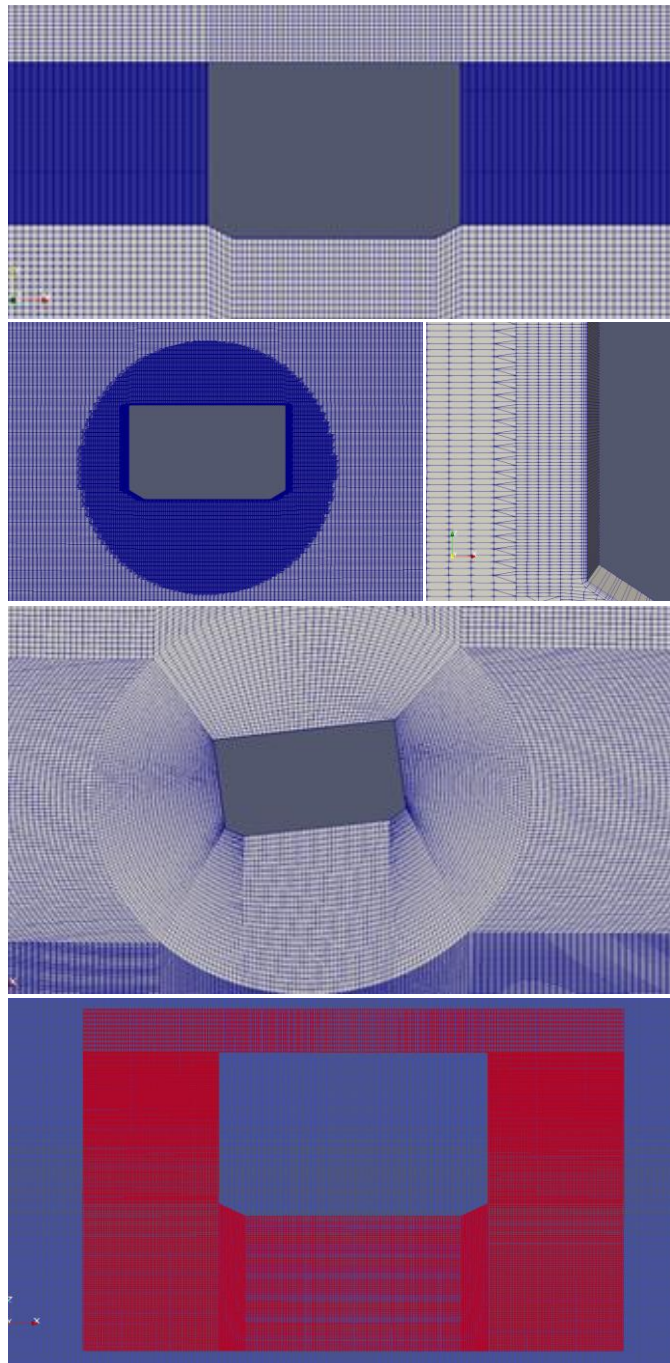
Figure 7. First plot: Simple block hex mesh. Second plot: Unstructured O mesh for the 2D intact section (left) with near-body details (right). Third plot: Structured O mesh. Fourth plot: Body-fitted OG in red and background OG in blue

At each time step, the hole and interpolation layer are updated, this leads to a computational overhead. In addition, the accuracy of the interpolation determines the effectiveness over deforming meshes. More details on the implementation of overset grids in OF can be found e.g. in Ma et al. [24].

To investigate further, the influence of numerical parameters and to analyze the importance of nonlinear *versus* viscous-flow effects, two in-house solvers are also used to simulate the fixed intact section in waves. They are outlined next.
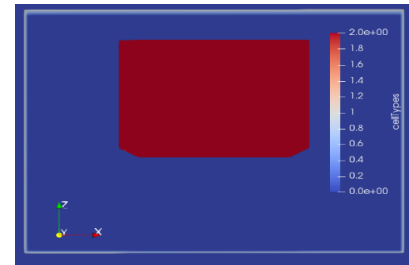

Figure 8. Hole and interpolation region for OG grid

3.2 In house NS solver
The fully nonlinear NSLS solver described in Colicchio et al. [13] is used for comparison. It uses a second order finite difference representation of the NS equations and a second order predictor-corrector scheme for the time integration. Both moving body surface and free-surface are represented with two level set functions that define the geometric distance of each point from those surfaces; this allows the use of a fixed rectangular grid to define the moving body and free surface. A local grid refinement is applied close to the wavemaker region, the free-surface region and the ship section. The use of the method helps to compare the LS and VOF free-surface techniques for the examined cases.

3.3 In house potential-flow BEM solver
The fully nonlinear BEM code described in Greco et al. [14]. is used with a flap wavemaker at one end and a numerical beach at the other end. A boundary value problem (BVP) is solved for the velocity potential, ϕ, at any time instant with a BEM using linear shape functions. The free-surface boundary conditions, with Lagrangian formulation, are stepped in time with a fourth-order Runge-Kutta scheme. To estimate wave-induced loads, the body pressure is obtained from the Bernoulli equation. The latter involves the time derivative of ϕ for which a similar BVP as for ϕ is solved. The diffraction-problem simulations are performed with a time step equal to 0.01T and with the same spatial discretization, corresponding to about 210 nodes per wavelength in the longest-wave case. These choices ensured converged results. The BEM use helps to compare the importance of nonlinear and viscous-flow effects for the examined cases.

4 RESULTS
4.1 Flapping foil
The case is studied in OF with DM and OG methods for one frequency and amplitude of oscillation, that should lead to a reverse von Karman wake and to a mean trust on the foil based on experiments [19]. The foil details are presented in figure 1. The inflow velocity U_c is calculated from the experimental chord-based Reynold's number set to Re$_c$=1173. The forced oscillation parameters are calculated from the experimental

Strouhal number (Sr=0.22) and the amplitude ratio A_D=1.77. Figure 9 presents a qualitative comparison for vorticity between the OF simulations with OG and the experiments. Euler method is used as temporal scheme and the ratio of outermost cell size of the overset grid to the background grid size (mesh ratio) is 1. We observe a reasonably similar behavior. The numerical simulation can capture the reverse von Karman vortex street quite well. The vortices, however, start to break up in the downstream of the foil. This effect is not captured in the simulations. It may be due to the time/space discretization causing diffusion or because of the linear interpolation scheme between overset and background grids. It can also be because we employed a laminar solver while the wake tends to become turbulent downstream of the body.
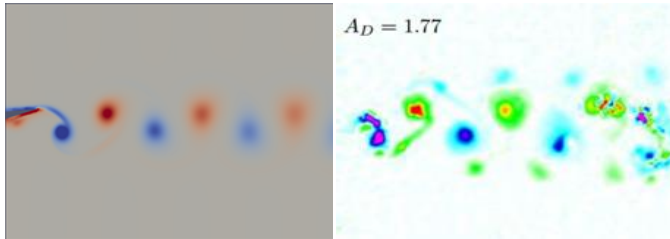

Figure 9. Vorticity from OF with OG (left) and experiments (right)

Figures 10 shows the vorticity for the simulated case using DM and OG techniques, respectively, with the same scale of the vorticity contour levels. The behavior is similar, but the intensity of vorticity is slightly lower for the deforming mesh, especially near the foil. Also, due to mesh deformation, the vortex structure for the DM case is not as smooth as the overset case. However, there is nearly a discontinuity for the overset grid near the outermost cell layer because of the interpolation between the overset and background grid. This is shown with a transparent circle.
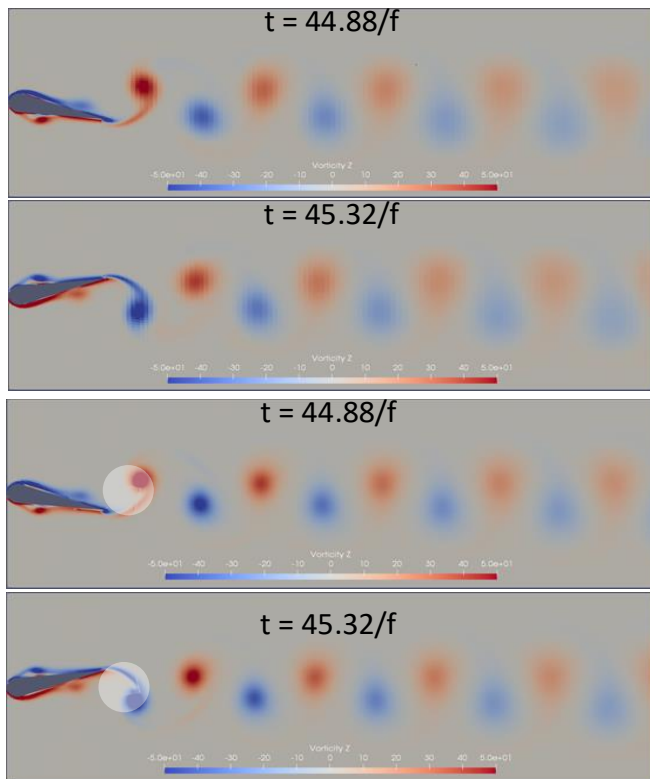

Figure 10. OF vorticity with DM (first two) and OG (bottom two)

To analyze the global effect of various parameters, the drag and lift coefficients, C_d and C_l, of the flapping foil are examined. Figure 11 shows the results for the two mesh motion types with Euler temporal scheme. As expected, the C_d frequency is twice the C_l frequency f. DM gives a much smoother behavior. One reason can be that the linear interpolation between grids in OG requires a smaller time step. Also, the troughs have slightly larger values for OG. The effect of mesh ratio and time schemes on the overset grid results are discussed in figure 12, in terms of C_d.
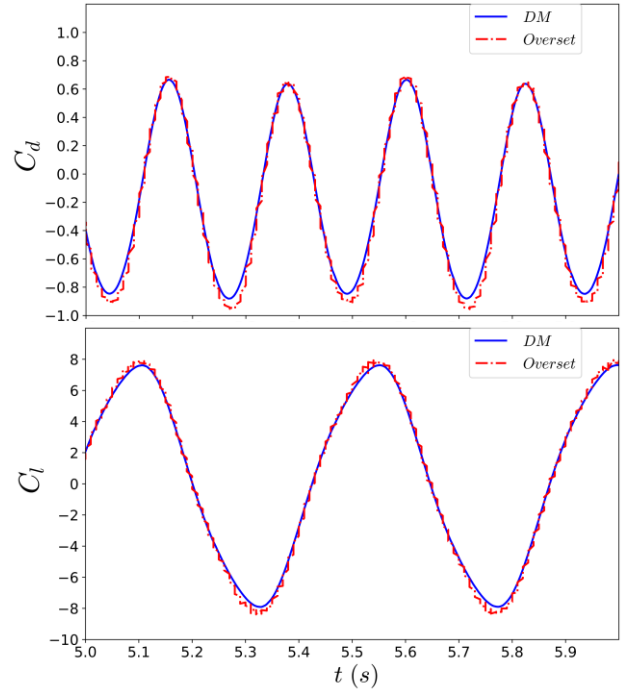

Figure 11. Flapping foil: Drag and lift coefficients vs time for DM and OG techniques
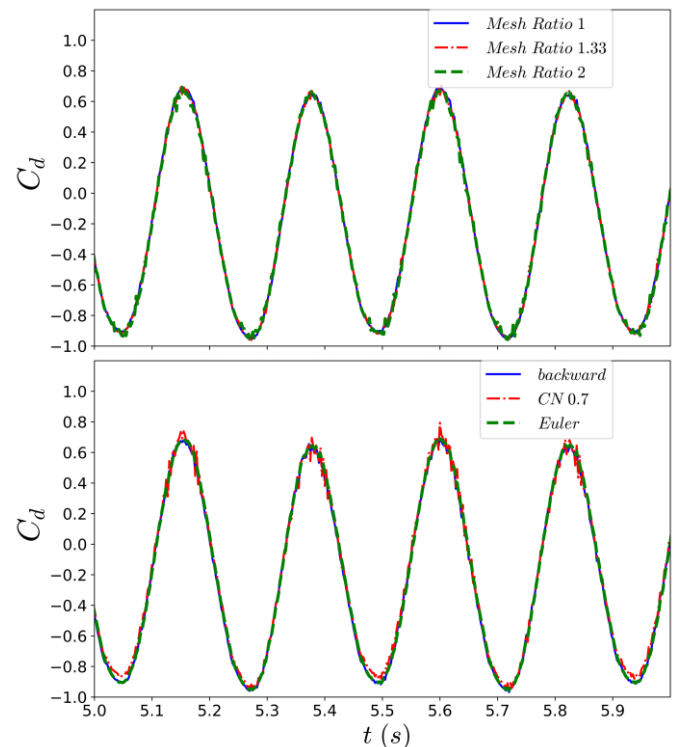

Figure 12. Drag coefficient for three mesh ratios (top) and three time schemes (bottom)

In the analysis of the mesh-ratio effect, Euler scheme is used for temporal discretization. Because OF allows only linear interpolation between grids in OG, it is important to keep the interpolation layer of the overset grid with very similar size as the background grid. This may lead to high computational costs and mesh generation issues sometimes but seems to give the most reliable results. For the time schemes, the Crank Nicolson (CN) method with an under-relaxation $\gamma=0.7$ produces some spikes both in C_d and C_l (not shown). The backward scheme is closer to the Euler method and both are much smoother compared to CN.

Table 1 discusses the average values of C_d and C_l during five oscillation periods. The negative value of C_d indicates thrust, which was the aim of the flapping foil studies. In general, all numerical cases show similar results for C_d. The maximum difference in C_d is for the mesh motion technique and is around 13%. The C_l values show more variation, almost for all parameters, a difference of 30% is observed. This study is useful to identify the solution sensitivity to the numerical parameters for a submerged foil case. Though, it may not be applicable to all cases in general. The flapping-foil experiments in [19] do not provide the time histories of the body loads. They document the mean drag coefficient, C_d, normalized by value for the non-flapping foil at zero angle of attack, C_{d0}. For the case examined here, with $Sr=0.22$ and $A_D=1.77$, the experiments document $C_d/C_{d0} = -0.6$. Numerically, using OG, we obtain $C_d/C_{d0} = -1$.

Table 1. Drag and lift coefficients *versus* numerical parameters

	C_d	C_l
Time Scheme		
backward scheme	-0.18	-0.15
CN 0.7	-0.16	-0.21
Euler	-0.17	-0.16
Mesh ratio		
1	-0.17	-0.16
1.33	-0.18	-0.12
2	-0.18	-0.11
Mesh Motion		
Overset	-0.17	-0.16
DM	-0.15	-0.11

4.2 Ship section

Here, an intact/damaged ship section is investigated as fixed in regular waves and then in prescribed oscillatory heave and roll motion in calm water.

4.2.1 Diffraction problem

The diffraction problem is examined simulating a moving boundary at the left end for generating waves, a fixed intact/damaged 2D section and a beach at the far end on the right side (fig. 5). A detailed analysis is given for wave period T=1s and wave steepness kA=0.033. The beam to draft (T_d) ratio for the intact section experiments and simulations is $B/T_d=5.88$, i.e. the draft is equal to the freely floating draft (8.5 cm).

The mesh is a block hex grid (fine mesh) with discretization given in table 2. For the time scheme, we use the CN scheme with $\gamma=0.9$. We focus on the global forces induced on the fixed section and the local wave elevation at two wave probe locations (WP1 and WP4). This is important to analyze the effectiveness of the NWT implemented in OF for wave propagation cases. Figure 13 shows the heave force per unit length ($F_3=f_3/L$) on a fixed intact section from experiments, OF, BEM and NS solvers. f_3 is the total heave force and L is the length perpendicular to the cross-section.

Table 2. Intact section, diffraction: Mesh details

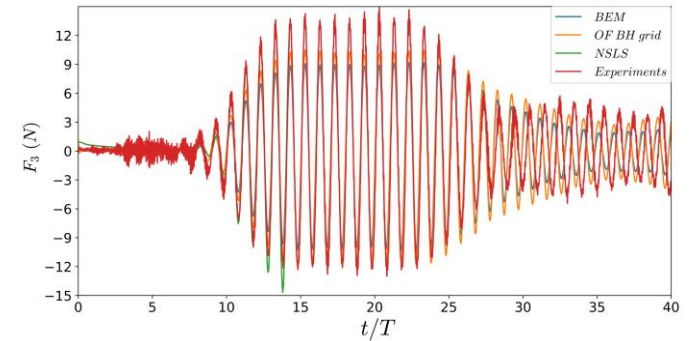|	$B/\Delta y$	$B/\Delta z$	$B/\Delta z$(near free-surface)
Coarse	25	50	100
Medium	50	50	100
Fine	50	50	200

Figure 13. Intact section, diffraction: Heave force from BEM, OF, NSLS and experiments

Reflections due to the flap wavemaker are evident after a steady state region (between 15–25 oscillations). The general agreement for all solvers with experiments in this steady state region is reasonable both for amplitude and phase of the heave force. A difference of 25% is observed between OF and experiments amplitude and the phase difference is negligible. The amplitude after 30 oscillations follows a similar behavior as earlier but the phase difference between the numerical solvers and experiments increases significantly. The phase and amplitude of the numerical solvers is almost same. This means that viscous effects are not large in this case as BEM neglects viscous effects.

To analyze the local wave elevation, we study that at WP1 and WP4 locations (figure 14). The behavior is similar, as for the force, between the numerical solvers and the experiments before the effect of wave reflections becomes evident. Since WP1 is closer to the wavemaker, the steady state region occurs earlier (between 8-18 oscillations). The numerical solvers display a similar behavior, which is more consistent with the experiments for WP4, but it is to be noted that the experimental data include considerable noise.

Figure 15 shows snapshots with streamlines from NSLS and OF solvers at two instants. Both results document no vortical structures near the body, confirming limited viscous-flow effects in this diffraction study. NSLS solver uses a LS function to define the body surface and therefore, we see a smooth distribution of streamlines near the body. For the OF case, a hex grid is used and the discretization near the body is fine close to the free surface but coarser towards the submerged part of the body. Thus, we observe differences especially there. This, however, does not affect global loads greatly in this case with fixed body and limited viscous-flow effects. In other parts of the fluid and near the free-surface, the behavior is quite similar. This study suggests that the body modeling in OF requires greater grid refinement. Attention should be paid when viscous effects and vortex shedding are involved.
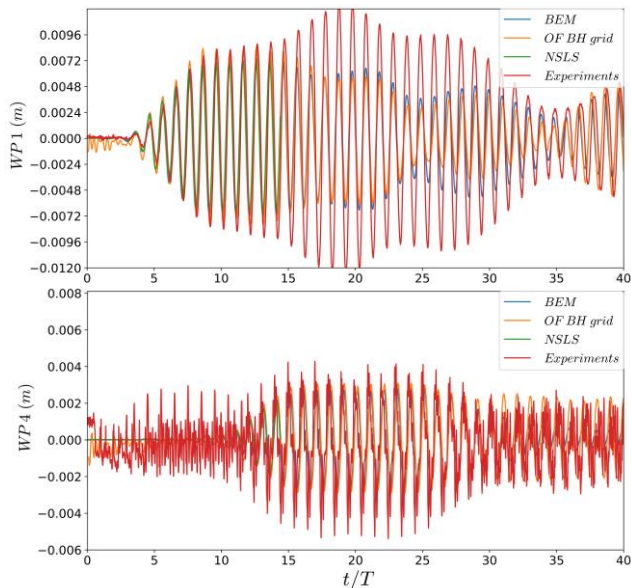
Figure 14. Intact section, diffraction: WP1 (top) and WP4 (bottom) values (location shown in fig. 3) from BEM, OF, NSLS and experiments
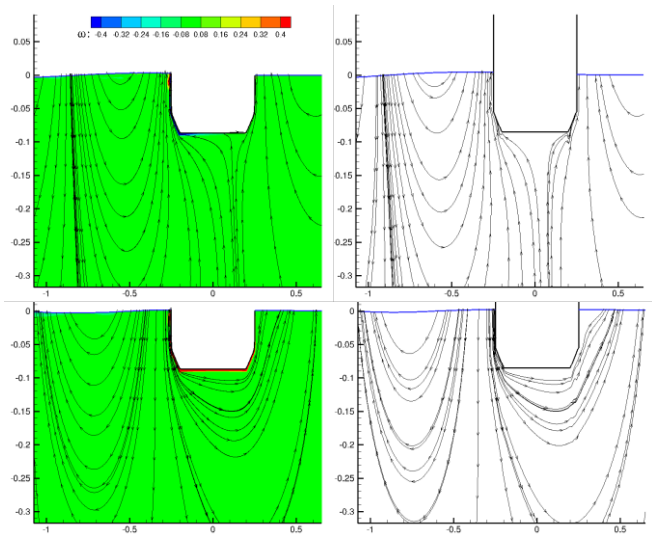

Figure 15. Intact section, diffraction: Streamlines from NSLS (left) and OF BH grid (right) at t/T=10.2 (top) and t/T=10.5 (bottom). For NSLS the vorticity (s⁻¹) field is also given

One of the most important factors controlling numerical diffusion in a NWT with propagating waves is the time discretization scheme. This effect is analyzed in figure 16 for heave force using the first-order Euler method and the second-order CN method with $\gamma=0.7$ and 0.9. From the results, the Euler scheme is highly diffusive, with a difference of 20% as compared with CN 0.9 scheme for the heave force. The CN scheme with 0.7 relaxation also shows a difference up to 10%. We chose CN 0.9 as the base scheme for all studied ship-section cases as it gave the results closest to the experimental data. Convergence analysis in space domain has been performed to ensure accuracy while limiting the computational costs. Here, we focus on the simple hex grid and systematically refine the grid. For the three studied grids (see table 2), heave-force results are in the top plot of figure 17. Overall the three mesh sizes show reasonable agreement. The difference between coarse and fine mesh is around 8% in the steady-state region, whereas it is

less than 3% between the medium and fine mesh. There is slight difference, though, in the beginning of the simulations. From this analysis, we can conclude that using the 'fine mesh' as a base mesh is appropriate to achieve converged values. We do not show the effect on local wave probe elevations since the discretization in z direction is the same for medium and fine grid and we do not expect a major difference.
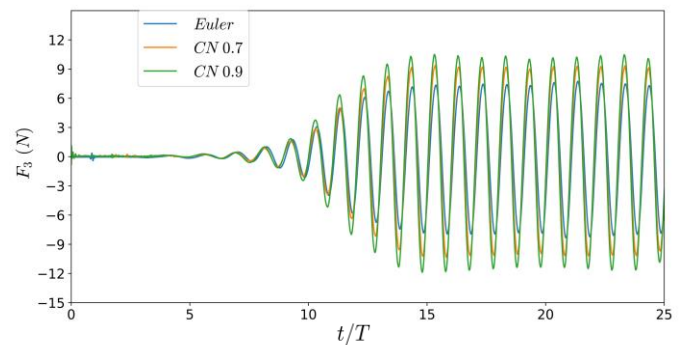

Figure 16. Intact section, diffraction: Heave force from OF (BH grid) with different time schemes
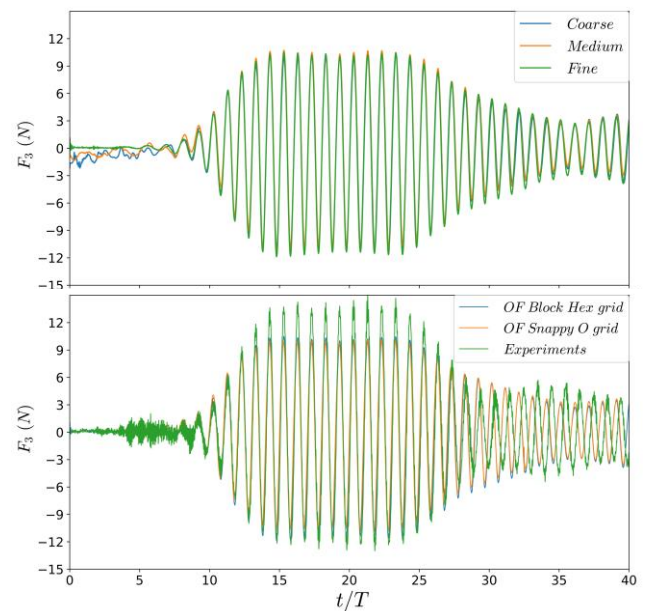

Figure 17. Intact section, diffraction: Heave force from OF with different sizes of block hex grid (top) and different grid types (bottom)

The bottom plot of figure 17 shows the comparison of the structured (hex) and unstructured (snappy) meshes on the heave force against the experiments. The O type snappy is highly refined near the body and the discretization is kept like the medium mesh for regions outside the body-centered O grid. For both cases the CN scheme with alpha 0.9 was used. The difference is almost negligible both in amplitude and phase for the two mesh types. The medium mesh outside the unstructured region ensures proper wave propagation. However, the time taken for the Snappy O grid simulation is almost 5 times higher due to highly refined region near the body causing Co stricter requirements. This highlights that a finer mesh does not always mean better results and an optimal simulation. On one hand, snappy mesh offers easy mesh generation with the user only required to input the geometry file of the body and relevant parameters, like number and size of surface layers, etc. On the other hand, a structured grid must be generated manually using available software or the *blockmesh* utility, but this provides a

more efficient computation. Therefore, mesh generation and mesh-type selection must be chosen wisely depending on individual scenarios to ensure an accurate and efficient simulation.

In the following, the diffraction problem for a damaged 2D section is examined with OF. In this case, the draft for the body is 15.5 cm (B/T_d=3.22) as in the experiments (the loading is same as for the intact section at 8.5 cm draft). We employ similar parameters as for the intact section, but now the block hex grid is also present inside the damaged section. Therefore, the number of cells increases slightly for this case. In the internal compartment, open to water, the discretization in x and z directions is set as near the free surface of the close external flow. The time scheme used is CN with γ=0.9. The incident wave periods vary between 0.8-2.3 s. To compare against the experiments, we must consider that the experimental 3D body has a damaged and an intact part (see figure 2). Therefore, numerically the diffraction force has also been calculated for a 2D intact section at same draft. Then, assuming valid a linear strip theory, we converted from 2D to 3D the numerical results using steady-state amplitude values (F_{3a}) as

$$F_{3a,dam,3D}=F_{3a,dam,2D}d+F_{3a,intact,2D}(L\text{-}d)$$ (1)

with L and d defined in figure 2. This numerical 3D force is compared with the experimental values in figure 18. OF captures the general trend but underestimates at most frequencies (less than 25%) with a maximum difference of 45%. This can be because the change in cross-section from damaged to intact can lead to relevant local 3D effects and make questionable the assumption of linear strip theory.
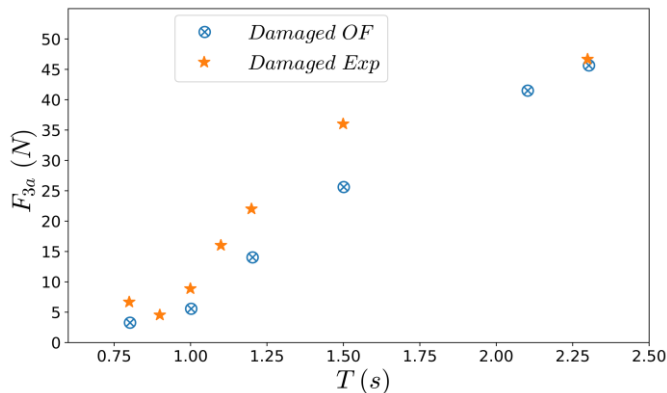

Figure 18. 3D damaged section, diffraction: Heave force from OF and experiments

4.2.2 Radiation problem

The radiation problem is solved using OF for a section forced to oscillate in heave in calm water. Both intact (B/T_d=5.88) and damaged (B/T_d=3.22) sections are examined with a forcing amplitude of 5 mm and angular forcing frequencies ω ranging from 2.73-7.85 rad/s. A block hex grid with discretization values equal to the fine mesh (table 2) is used for the intact case. In the damaged scenario, the internal damage compartment discretization is the same as for the diffraction case. For the time scheme, we use CN with γ=0.9 in both simulations. For the mesh motion due to heave, the DM described before is used. In this case, the motions are linear and relatively small, therefore even with mesh distortion, the general quality of the mesh is well-preserved. Heave added mass (a_{33}) and damping (b_{33}) for

a 2D intact and damaged section are calculated as in [15] and compared against the experiments in figure 19 using the following non-dimensional definition

$$a_{33}^*=\frac{a_{33}}{\rho A_r}:b_{33}^*=\frac{b_{33}}{\rho A_r}\sqrt{\frac{B}{2g}}:\omega^*=\omega\sqrt{\frac{B}{2g}}$$ (2)

OF captures the general trend for both added mass and damping and for both the intact and damaged sections. The maximum difference for added mass and damping of the intact section is 23% and 17%, respectively. The maximum difference for both added mass and damping of damaged section is around 30%.
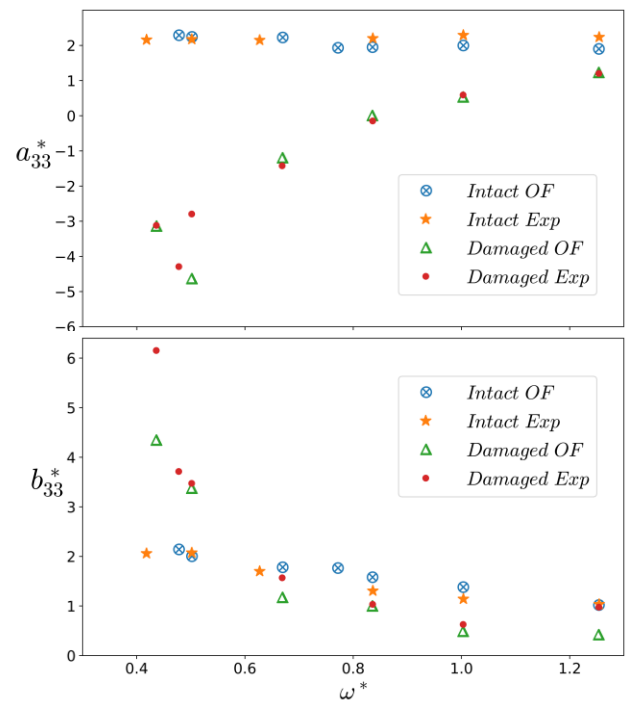

Figure 19. Intact and damaged sections, heave radiation: Added mass and damping from OF and experiments

As a last case, we examine forced roll motion of an intact section in calm water about the center of gravity (same as in the experiments, calculated from swing tests). 2D forced roll simulations can be important for midship sections where the cross-section remains almost constant for a certain length. This can especially help to assess roll damping due to bilge keels and optimize their design. The block hex grid used earlier cannot handle angular motions (see figure 20), so we use a structured O grid and a snappy O grid for DM simulations.

Structured O grid mesh quality is preserved well for an angle of 10° (figure 7, third plot). We also compare with an OG simulation. The OG grid will be used in future works for damaged-section roll motions, since DM cannot handle deformations in such a scenario. These simulations present an initial assessment on the use of OG grids for the simpler intact section. For the DM case, we use the CN 0.9 temporal scheme. For OG simulations, we use the Euler scheme due to computational restrictions. The mesh sizes for the body grid and background grid are the same as the medium mesh described earlier, except near the free surface region where the cell size is slightly larger, i.e. $B/\Delta z$=150. Figure 21 demonstrates roll moment measured about the center of gravity for the 2D intact section (for ω^*=1.25 and forced roll amplitude of 10°). We see

Copyright © 2020 ASME

that OG gives the smoothest results, as no mesh deformation occurs. Both structured and snappy O grids have significant deformations causing spikes, especially for the snappy mesh. The difference for time-averaged moment (2-4 oscillations) between snappy and OG results is around 20% with a similar computational time. For the structured grid, the difference is ~25% but the time required is ten times smaller. Figure 22 shows the vorticity field at the same time instant from an OG simulation and a DM snappy O grid. For the OG case, the intensity of vorticity is smaller, especially away from the body. This is due to a lower vorticity generation at the edges that is dissipated by a lower order time integration scheme. The mesh deformation in snappy grid results in more disturbances near the free-surface as compared to the OG case. The vorticity close to the body surface is similar in both cases with a finer resolution for OG.
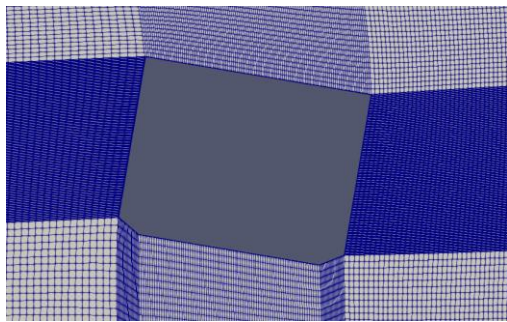

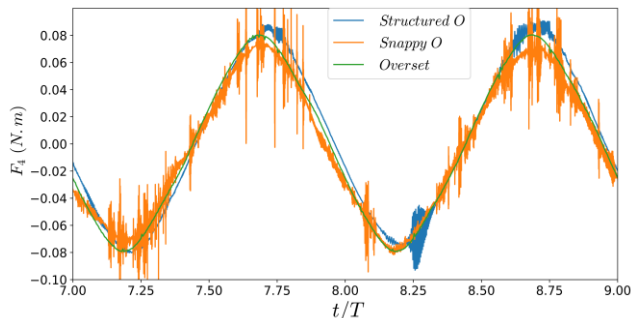**Figure 20.** Intact ship, forced roll: Severely deformed BH grid

Figure 21. Intact ship, forced roll: Roll moment for OF with Structured O grid, Snappy O grid and OG
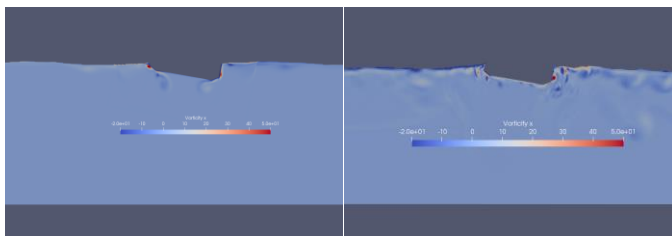

Figure 22. Intact ship, forced roll: Vorticity (s^{-1}) field in OG (left) and Snappy O grid (right) at t/T=8.75

5 NUMERICAL ERROR SOURCES

Here, we do not present quantitative results on order of accuracy and detailed convergence analysis. We must, however, list the error sources and uncertainties. For a CFD solver, they are due to simplification of the physical problem, for example modelling of the free surface using a LS or VOF technique, and due to the numerical discretization of the field equations. For example, the Euler method is only first order accurate and cannot be used to model long-time nonlinear problems.

6 CONCLUSIONS

Two complex hydrodynamic problems are analyzed– a submerged flapping foil in uniform inflow and an intact/damaged ship section fixed in regular waves, and in forced oscillatory heave and roll motion in calm water, with focus on assessment of numerical results from open-source solver OpenFOAM using benchmark and in-house experiments. For the diffraction problem of an intact section, the NWT in OF is compared against an in-house BEM and NS solver with an overall good agreement, confirming negligible viscous effects. Experimental data have in general their own uncertainties [15]. Nevertheless, for most of the studied cases, we obtain reasonable agreement for OF with experiments. In addition, effect of parameters such as mesh type, mesh size, time schemes and mesh motion techniques on the results has been analyzed in detail. Both single/two phase solvers are studied. This analysis can help researchers to make suitable choices for similar problems, especially in relation to OF simulations.

ACKNOWLEDGEMENT

REFERENCES

[1] Jacobsen, N.G., Fuhrman, D.R., and Fredsoe, J. (2012). A wave generation toolbox for the open-source CFD library: OpenFoam (R). *Int J Numer Methods Fluids*, *70(9), 1073–108.*

[2] Bihs, H., Kamath, A., Chella, M.A., Aggarwal, A., and Arntsen, Ø.A., (2016). A new level set numerical wave tank with improved density interpolation for complex wave hydrodynamics. *Computers & Fluids,140 (191-208).*

[3] Windt, C., Davidson, J., Schmitt, P., and Ringwood, J.V., (2019). On the Assessment of Numerical Wave Makers in CFD Simulations. *Journal of Marine Science and Engineering. 2019, 7, 47.*

[4] Miquel, A.M., Kamath, A., Chella, M.A., Archetti, R., and Bihs, H., (2018). Analysis of Different Methods for Wave Generation and Absorption in a CFD-Based Numerical Wave Tank. *Journal of Marine Science and Engineering. 6. 73.*

[5] Bonfiglio, L., Brizzolara, S., and Chryssostomidis, C., (2011). Added mass and damping of oscillating bodies: a fully viscous numerical approach. *Recent Advances in Fluid Mechanics, Heat & Mass Transfer and Biology, 210-215*

[6] Chen, H., and Christensen, E.D., (2016). Computation of added mass and damping coefficient of a horizontal circular cylinder in OpenFOAM. *Proceedings of the 35th International Conference on Ocean, Offshore and Arctic Engineering.*

[7] Thilleul, O., Babarit, A., Drouet, A., and Le Floch, S., (2013). Validation of CFD for the Determination of Damping Coefficients for the Use of Wave Energy Converters Modelling. *Proceedings of the 32nd International Conference on Ocean, Offshore and Artic Engineering.*

[8] Jaouen, F., Koop, A., and Vaz, G., (2011). Predicting Roll Added Mass and Damping of a Ship Hull Section Using CFD. *Proceedings of the 30th International Conference on Ocean, Offshore and Arctic Engineering.*

[9] Mancini, S., Begovic, E., Day, A.H., and Incecik, A., (2018). Verification and validation of numerical modelling of DTMB 5415 roll decay. *Ocean Engineering, 162, (209-223).*

[10] Windt, C., Davidson, J., Akram, B., and Ringwood, J. V. (2018). Performance Assessment of the Overset Grid Method for Numerical Wave Tank Experiments in the OpenFOAM Environment. *Proceedings of the 37th International Conference on Ocean, Offshore and Arctic Engineering.*

[11] Decorte, G., and Monbaliu, J. (2018). A Review on the Application of OpenFOAM's Mesh Motion Techniques to Wave-Structure Interaction Problems. *Proceedings of the 21st Numerical Towing Tank Symposium.*

[12] Chen, H., Qian, L., Ma, Z., Li, Y., Causon, D., and Mingham, C. (2019). Application of an overset mesh based numerical wave tank for modelling realistic free-surface hydrodynamic problems. *Ocean Engg.*

[13] Colicchio, G., Landrini, M., and Chaplin, J., (2005). Level-set computations of free surface rotational flows. *Journal of Fluids Engineering;127(6):1111–1121.*

[14] Greco, M., Faltinsen, O.M., and Landrini, M., (2005). Shipping of Water on a Two-dimensional Structure, *J. of Fluid Mechanics, 525.*

[15] Siddiqui, M.A., Greco, M., Faltinsen, O.M. and Lugni, C. (2019). Experimental studies of a damaged section in forced heave motion. *Applied Ocean Research 88.*

[16] Triantafyllou, G.S., Triantafyllou, M.S., and Grosenbaugh, M.A., (1993). Optimal thrust development in oscillating foils with application to fish propulsion. *Journal of Fluids and Structures, 7(2), 205-224.*

[17] Andersen, A., Bohr, T., Schnipper, T., and Walther, J.H., (2017). Wake structure and thrust generation of a flapping foil in two-dimensional flow. *Journal of Fluid Mechanics, 812.*

[18] Lampropoulos, N., Koubogiannis, D., Belibassakis, K., and Street, A.S., (2016). Numerical simulation of flapping foil propulsion. *11th HSTAM International Congress on Mechanics Athens.*

[19] Godoy-Diana, R., Aider, J.L., and Wesfreid, J.E., (2008). Transitions in the wake of a flapping foil. *Phys. Rev. E 77, 016308.*

[20] Begovic, E., Day, A.H., Incecik, A., Mancini, S., and Pizzirusso, D., (2015). Roll Damping Assessment of Intact and Damaged Ship by CFD and EFD Methods. *Proceedings of the 12th International Conference on the Stability of Ships and Ocean Vehicles.*

[21] OpenFOAM® v1806: OpenFOAM Documentation *https://www.openfoam.com/releases/openfoam1806/documentation.php*

[22] Higuera, P., Lara, J. L., and Losada, I. J. (2013). Realistic wave generation and active wave absorption for Navier-Stokes models. Application to OpenFOAM®. *Coast Eng, 71, 102–118.*

[23] Jasak, H., and Tukovic, Z., (2006). Automatic mesh motion for the unstructured Finite Volume Method. *Transactions of FAMENA. 30. 1-20.*

[24] Ma, Z. H., Qian, L., Martinez-Ferrer, P. J., Causon, D. M., Mingham, C., and G., Bai, W. (2018). An overset mesh based multiphase flow solver for water entry problems. *Computer and Fluids*, 172 (689-705).